# An Adjoint-based Topology Optimization Framework for Fluid Mechanics and Conjugate Heat Transfer in OpenFOAM

E.M. Papoutsis-Kiachagias[1], K.C. Giannakoglou[2]

[1] *Researcher, PhD, e-mail:vpapout@mail.ntua.gr*
[2] *Professor, e-mail:kgianna@mail.ntua.gr, web page:http://velos0.ltt.mech.ntua.gr/research/*
*Parallel CFD & Optimization Unit*
*National Technical University of Athens (NTUA)*
*9, Heroon Polytechniou, NTUA Zografou Campus, 15780, Athens, Greece*

## Abstract

This paper presents recent developments pertaining to an adjoint-based topology optimization software for aero/hydrodynamic and conjugate heat transfer problems, based on the adjoint infrastructure of OpenFOAM v1912/v2006. The software follows the density (porosity)-based approach, incorporating recent developments related to the regularization and projection of the underlying porosity field. The flow and adjoint equations along with the topology optimization problem formulation are presented in brief, followed by academic and industrial applications.

## 1 Introduction

Topology Optimization (TopO) is nowadays a popular method for the preliminary design of industrial duct systems with multiple inlets and outlets [7]. Though a number of variants exist for formulating the TopO problem, such as the density- (or porosity) based approach [3] or level-set methods [4], they all follow the idea of artificially blocking part of an initial flow domain to penalize its counter-productive areas, in an attempt to minimize an objective function $J$, such as the total pressure losses between the inlets and outlets of the domain. This blockage (or porosity) field acts as the field of the design variables in TopO problems. Usually, one design variable exists per grid cell, formulating optimization problems with thousands or millions of design variables. This particular feature of TopO makes the utilization of adjoint methods for computing the gradient of $J$ with respect to (w.r.t.) the design variables $\alpha_n, n \in [1, N]$ the only computationally feasible approach.

Since v1906, OpenFOAM includes an extensive library for solving the continuous adjoint equations for incompressible, turbulent flows which was enhanced with a framework for automated shape optimization loops in v1912. This paper presents an extension of this framework to solve TopO problems, covering incompressible fluid dynamics and conjugate heat transfer (CHT). The method and software rely on the density-based TopO approach [3], properly formulated to cover incompressible turbulent flows, by enhancing the mean flow, turbulence and distance equations with porosity-dependent terms. Additionally, the energy equation (and its adjoint) are solved

to take into consideration CHT effects, by interpolating the thermo-physical properties between the fluid and solid domains using the porosity field containing the design variables of the TopO problem. The TopO approach, including the primal and adjoint equations, as well as a number of recent developments such as the regularization of the porosity field to mitigate the effects of a grid-dependent solution and the checkerboard effect [5], is presented in brief in section 2. Then, the developed software is used to tackle some academic and industrial cases in section 3.

# 2 TopO problem formulation

In TopO problems, the field of design variables $\alpha$ is used to solidify the part of the initial flow domain that is counter-productive w.r.t. the objective function $J$ that needs to be minimized. Parts of the computational domain with an (almost) unitary $\alpha$ value correspond to the solidified areas whereas practically zero $\alpha$ values indicate the fluid part of the domain. The interface between the two regions indicates the designed walls of the duct system. To simulate the solidification of parts of the computational domain, the flow equations are augmented with $\alpha$-dependent source terms, locally driving the flow solution towards values corresponding to solid boundaries. The altered flow equations, coupled with the Spalart-Allmaras [9] one-equation turbulence model PDE and the Eikonal equation to compute the distance $\Delta$ from the walls, as well as the energy equation read

$$R^p = -\frac{\partial v_j}{\partial x_j} = 0 \tag{1a}$$

$$R_i^v = v_j \frac{\partial v_i}{\partial x_j} - \frac{\partial \tau_{ij}}{\partial x_j} + \frac{\partial p}{\partial x_i} + \beta_{max} I^v(\beta) v_i = 0 \ , \qquad i = 1, 2(, 3) \tag{1b}$$

$$R^{\widetilde{\nu}} = v_j \frac{\partial \widetilde{\nu}}{\partial x_j} - \frac{\partial}{\partial x_j}\left[\left(\nu + \frac{\widetilde{\nu}}{\sigma}\right)\frac{\partial \widetilde{\nu}}{\partial x_j}\right] - \frac{c_{b2}}{\sigma}\left(\frac{\partial \widetilde{\nu}}{\partial x_j}\right)^2 - \widetilde{\nu} P(\widetilde{\nu}) + \widetilde{\nu} D(\widetilde{\nu}) + \beta_{max} I^{\widetilde{\nu}}(\beta)\widetilde{\nu} = 0 \tag{1c}$$

$$R^{\Delta} = \frac{\partial}{\partial x_j}\left(\frac{\partial \Delta}{\partial x_j}\Delta\right) - \Delta\frac{\partial^2 \Delta}{\partial x_j^2} - 1 + \beta_{max} I^{\Delta}(\beta)\Delta = 0 \tag{1d}$$

$$R^T = (1-\beta)\rho c_p \frac{\partial (v_j T)}{\partial x_j} - \frac{\partial}{\partial x_j}\left[k(I^k(\beta))\frac{\partial T}{\partial x_j}\right] = 0 \tag{1e}$$

where $\beta \in [0, 1]$ is a field that depends on the porosity field $\alpha$ (see below) and shares its physical interpretation, $v_i$ are the velocity components, $p$ is the pressure divided by the fluid density, $\tau_{ij} = (\nu + \nu_t)\left(\frac{\partial v_i}{\partial x_j} + \frac{\partial v_j}{\partial x_i}\right)$, $\nu$ and $\nu_t$ are the bulk and eddy viscosity coefficients respectively and $P(\widetilde{\nu})$ and $D(\widetilde{\nu})$ are the production and dissipation terms of the turbulence model, respectively, [9]. Additionally, $T$ is the temperature field, $\rho$ and $c_p$ the constant fluid density and specific heat transfer coefficient under constant pressure, respectively, and $k$ the thermal conductivity, interpolated between the fluid and the solidified parts of the domain. Furthermore, the $I^v, I^{\widetilde{\nu}}, I^{\Delta}, I^k$ functions are used to either drive the flow solution towards values corresponding to solid walls (eqs. 1b to 1d) or to interpolate between the thermo-physical properties of the fluid and solidified domains (eq. 1e). In eq. 1e, the convection term is multiplied with $(1-\beta)$ to cancel out the inevitable small-scale leakage of fluid into the solid domain that is almost always observed in TopO. The $\beta_{max}$ value is used to ensure that the $v_i, \widetilde{\nu}$ and $\Delta$ values are practically zero in the solidified domain. Its value can be computed based on the Darcy number, quantifying the ratio between viscous and porous forces, [6],

$$Da = \frac{\nu}{\beta_{max} L^2} \tag{2}$$

where $L$ is a characteristic length of the case under consideration. In all cases presented in section 3, $Da = 10^{-5}$ and $L$ is either the inlet length or the inlet hydraulic diameter for $2D$ and $3D$ cases,

respectively. The porosity-dependent terms added to eqs. 1b to 1d as well as the $k$ interpolation in eq. 1e are implemented as new *fvOptions*, to allow for code modularity and adaptability. A number of $I$ functions have been proposed in the literature and implemented into the software. Here, only the ones used in section 3 are mentioned, namely the one proposed by Borrvall and Petersson in [2] and the Solid Isotropic Material with Penalization (SIMP) [1], i.e.

$$I_{B-P}(\beta) = \frac{\beta}{1 + b(1-\beta)} \tag{3a}$$

$$I_{SIMP}(\beta) = \beta^b \tag{3b}$$

where $b$ is a parameter controlling the steepness of the interpolation function. Larger $b$ values correspond to sharper distinctions between the fluid and solid domains. However, larger $b$ values also lead to stiffer optimization problems. Hence, the software offers the capability of varying the $b$ values throughout the optimization cycles using any of the available *Function1* schemes, including an additional *step* one that increases the $b$ value in a stepped manner, after a prescribed number of optimization cycles. Therefore, $b$ values in the order of 1 are usually used in the first few optimization cycles and gradually increased to a range of $3 - 10$ to obtain a sharp interface between the fluid and solid domains.

In a number of TopO problems, especially those related to CHT, checkerboard artifacts may appear in the $\alpha$ field. To avoid these artifacts and to mitigate the effects of local grid size to the optimized solution, the so-called regularization of the porosity field can be performed [5]. Here, this is implemented through the use of a Helmholtz-type filter [5], i.e.

$$-r^2 \frac{\partial^2 \widetilde{\alpha}}{\partial x_j^2} + \widetilde{\alpha} = \alpha \tag{4}$$

where $\widetilde{\alpha}$ is the regularized porosity field and $r$ can be seen as a smoothing radius, usually computed as a function of the average grid cell size. Regularization, as any other smoothing technique, unavoidably blurs the line between the fluid and solidified domains. To increase the contrast of the $\widetilde{\alpha}$ field, a so-called projection can follow the regularization step, using the following relation [5]

$$\beta = \frac{tanh(0.5b) + tanh[b(\widetilde{\alpha} - 0.5)]}{2tanh(0.5b)} \tag{5}$$

where $b$ is a sharpening parameter, similar to that met in eq. 3. If no regularization/projection is applied, $\beta = \alpha$ in eqs. 1.

After following the methodology outlined in [8], the continuous adjoint PDEs to eqs. 1 can be

developed and read

$$R^q = -\frac{\partial u_j}{\partial x_j} = 0 \tag{6a}$$

$$R^u_i = u_j \frac{\partial v_j}{\partial x_i} - \frac{\partial (v_j u_i)}{\partial x_j} - \frac{\partial \tau^\alpha_{ij}}{\partial x_j} + \frac{\partial q}{\partial x_i} + \widetilde{\nu_a} \frac{\partial \widetilde{\nu}}{\partial x_i} - \frac{\partial}{\partial x_l} \left( \widetilde{\nu_a} \widetilde{\nu} \frac{C_Y}{Y} e_{mjk} \frac{\partial v_k}{\partial x_j} e_{mli} \right)$$
$$+ \rho c_p \left\{ (1-\beta) T_a \frac{\partial}{\partial x_j} \left( \frac{\partial T}{\partial x_j} \right) - \frac{\partial}{\partial x_j} \left[ (1-\beta) T_a \frac{\partial T}{\partial x_j} \right] \right\} + \beta_{max} I^v(\beta) u_i = 0 \quad i = 1, 2(, 3) \tag{6b}$$

$$R^{\widetilde{\nu_a}} = -\frac{\partial (v_j \widetilde{\nu_a})}{\partial x_j} - \frac{\partial}{\partial x_j} \left[ \left( \nu + \frac{\widetilde{\nu}}{\sigma} \right) \frac{\partial \widetilde{\nu_a}}{\partial x_j} \right] + \frac{1}{\sigma} \frac{\partial \widetilde{\nu_a}}{\partial x_j} \frac{\partial \widetilde{\nu}}{\partial x_j} + 2 \frac{c_{b2}}{\sigma} \frac{\partial}{\partial x_j} \left( \widetilde{\nu_a} \frac{\partial \widetilde{\nu}}{\partial x_j} \right) + \widetilde{\nu_a} \widetilde{\nu} C_{\widetilde{\nu}}$$
$$+ \frac{\partial \nu_t}{\partial \widetilde{\nu}} \frac{\partial u_i}{\partial x_j} \left( \frac{\partial v_i}{\partial x_j} + \frac{\partial v_j}{\partial x_i} \right) + (-P + D) \widetilde{\nu_a} + \beta_{max} I^{\widetilde{\nu}}(\beta) \widetilde{\nu_a} = 0 \tag{6c}$$

$$R^{\Delta_\alpha} = -2 \frac{\partial}{\partial x_j} \left( \Delta_\alpha \frac{\partial \Delta}{\partial x_j} \right) + \widetilde{\nu} \widetilde{\nu_a} C_\Delta + \beta_{max} I^\Delta(\beta) \Delta_\alpha = 0 \tag{6d}$$

$$R^{T_\alpha} = -\rho c_p \frac{\partial}{\partial x_j} [(1-\beta) v_j T_a] - \frac{\partial}{\partial x_j} \left[ k(I^k(\beta)) \frac{\partial T_a}{\partial x_j} \right] = 0 \tag{6e}$$

where $u_i$ are the adjoint velocity components, $q$ the adjoint pressure, $\widetilde{\nu_a}$ the adjoint to the turbulence model variable, $\tau^\alpha_{ij} = (\nu + \nu_t) \left( \frac{\partial u_i}{\partial x_j} + \frac{\partial u_j}{\partial x_i} \right)$ are the adjoint stresses, $\Delta_\alpha$ the adjoint distance from the walls and $T_\alpha$ the adjoint temperature field. Terms $C_{\widetilde{\nu}}$, $C_Y$ and $C_\Delta$ can be found in [12]. The adjoint boundary conditions can be developed by following the methodology outlined in [8] and are omitted in the interest or brevity.

After solving the primal and adjoint PDEs, the sensitivity derivatives w.r.t. the $\alpha$ field can be computed as

$$\frac{\delta J}{\delta \widetilde{\alpha}} = \int_\Omega \left[ \beta_{max} \left( v_i u_i \frac{\partial I^v}{\partial \beta} + \widetilde{\nu} \widetilde{\nu_a} \frac{\partial I^{\widetilde{\nu}}}{\partial \beta} + \Delta \Delta_a \frac{\partial I^\Delta}{\partial \beta} \right) - \rho c_p T_a \frac{\partial (v_j T)}{\partial x_j} \right] \frac{\partial \beta}{\partial \widetilde{\alpha}} d\Omega$$
$$+ \int_\Omega \left[ \frac{\partial}{\partial x_j} \left( T_a \frac{\partial T}{\partial x_j} \right) - T_a \frac{\partial^2 T}{\partial x_j^2} \right] \frac{\partial k}{\partial \beta} \frac{\partial \beta}{\partial \widetilde{\alpha}} d\Omega \tag{7a}$$

$$R^{\Psi_{\widetilde{\alpha}}} = -r^2 \frac{\partial^2 \Psi_{\widetilde{\alpha}}}{\partial x_j^2} + \Psi_{\widetilde{\alpha}} - \frac{\delta J}{\delta \widetilde{\alpha}} = 0 \tag{7b}$$

$$\frac{\delta J}{\delta \alpha} = \Psi_{\widetilde{\alpha}} \tag{7c}$$

where $\partial \beta / \partial \widetilde{\alpha}$ is computed analytically by differentiating eq. 5 and eq. 7b is the adjoint to the regularization equation. In case no regularization is employed, $\delta J / \delta \alpha$ is given directly by eq. 7a.

Two objective functions are used in the cases that follow in section 3, the total pressure losses between the inlet(s) $S_I$ and the outlet(s) $S_O$ of the fluid domain

$$J_{p_t} = -\int_{S_I, S_O} \left( p + \frac{1}{2} v_k^2 \right) v_i n_i dS \tag{8}$$

to be minimized and the heat flux difference between $S_I$ and $S_O$

$$J_Q = \int_{S_I, S_O} v_j n_j T dS \tag{9}$$

to be maximized. Additionally, as is accustomed to TopO problems, an inequality constraint related to the percentage of the computational domain occupied by the fluid is also included in all applications of section 3, formulated as

$$C_V = \frac{\int_\Omega (1-\beta) d\Omega}{\int_\Omega d\Omega} - t < 0 \tag{10}$$

where $t$ is the target fluid volume percentage.

After computing the objective and constraint derivatives, the $\alpha$ field is updated using the Method of Moving Asymptotes (MMA) [10] or its Globally Convergent variant (GCMMA) [11], both of which have been programmed into OpenFOAM. (GC)MMA can handle inequality constraints as well as bounds for the design variables, both useful features for taking into consideration the constraint of eq. 10 and the fact that the $\alpha$ field should lay in the $[0, 1]$ range.

# 3 Applications

This section presents some applications of the method and software outlined in section 2, for pure aerodynamic as well as CHT TopO problems.

The first two problems presented herein were initially studied in [4] using a level-set TopO approach. They are re-visited here in order to have a measure of comparison for the newly developed features presented in section 2. Fig. 1 depicts the TopO of a duct system with one inlet and two outlets. The Reynolds number based on the inlet height is $Re = 200$ and $J_{p_t}$ is minimized under the volume constraint defined by eq. 10 with $t = 0.462$. No regularization was used in this case since no checkerboard effect was observed and $I^v(\beta) = \beta = \alpha$ was used in the momentum equations. For this and most of the other applications of this section, it was observed that activating the design variables gradually, starting from the initial walls of the computational domain and marching inwards a few cells in each optimization cycle, instead of letting them all change from the first optimization cycle, prevented the algorithm from being entrapped into a locally optimal solution of the multi-modal design space (10000 design variables) during the first few iterations of the TopO problem. Hence, the method shares some characteristics with level-set in the first optimization cycles (the optimal solution can march a few cells at a time, starting from the initial walls) and gradually switches to a typical density-based approach where all design variables can change simultaneously as the optimization cycles progress. $J_{p_t}$ was reduced by $\sim 33\%$ and the volume inequality constraint was satisfied ($C = -1.15 \times 10^{-7}$). A process for converting the TopO solution to a CAD-compatible description, re-meshing and evaluating using a body-fitted mesh has been developed by the authors and described in [4] but was considered outside the scope of this paper.

Fig. 2 presents the TopO solution of another problem initially studied in [4] with the level-set approach. The Reynolds number based on the inlet height is $Re = 200$ and $J_{p_t}$ is minimized under the volume constraint defined by eq. 10 with $t = 0.415$. No regularization was used in this case either. $J_{p_t}$ was actually increased by a small percentage (2.8%) in order to meet the imposed volume constraint. As with the first case studied, the optimized solution bears a lot of similarities with the level-set solution presented in [4], suggesting that the two methods can be used almost interchangeably.

In fig. 3, the TopO of a 3D manifold system is presented. The flow is laminar with a Reynolds number based on the inlet hydraulic diameter of 2000 and $J_{p_t}$ is minimized, under the $C_V$ constraint with $t = 0.3$. $J_{p_t}$ was reduced by $\sim 45\%$ and the fluid volume has been reduced significantly more than its supplied maximum value ($C = -0.054$).

Fig. 4, showcases the TopO of a Heating, Ventilation and Air-Conditioning (HVAC) duct located in a passenger car. The case was shared by Volkswagen AG in the context of the EU-funded

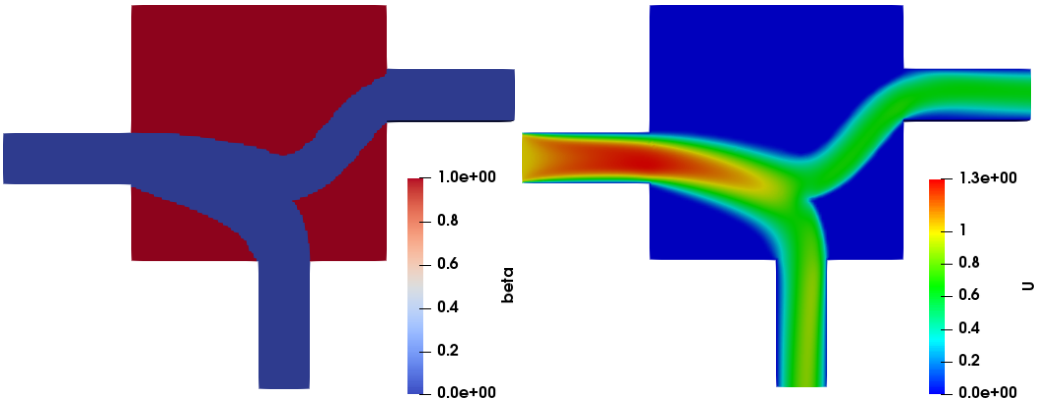


Figure 1: Case 1, One-inlet, two-outlet duct. The flow enters the domain from the left and exits from the bottom and right. The optimized $\beta$ field is shown on the left, where a binary distribution can be observed. The corresponding velocity magnitude is depicted on the right.

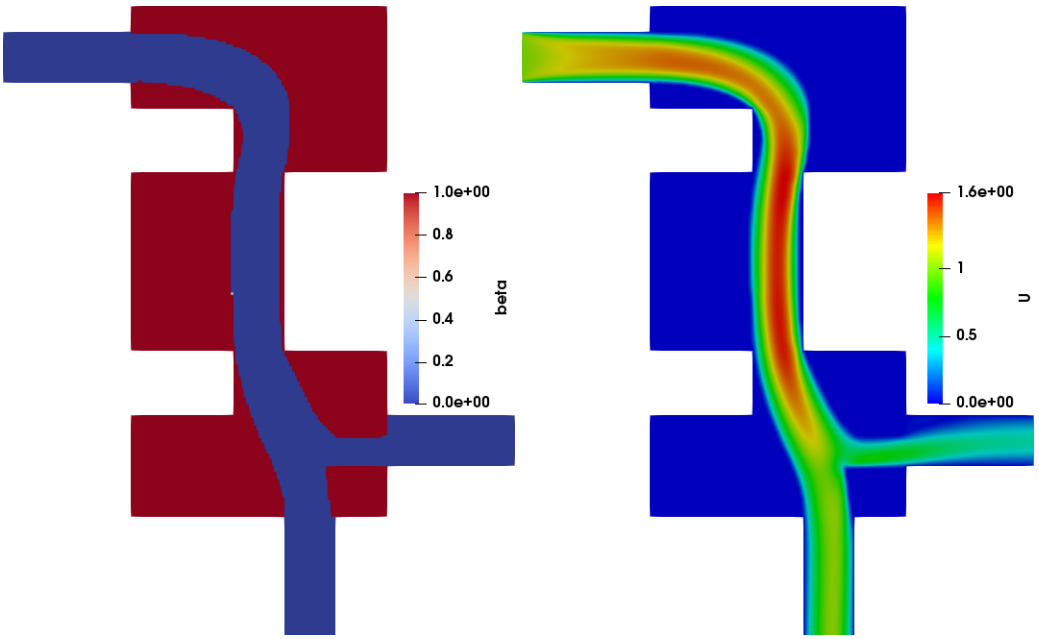


Figure 2: Case 2, One-inlet, two-outlet duct with a bottleneck formation. The flow enters the domain from the top left and exits from the bottom and right. The optimized $\beta$ field is shown on the left and the corresponding velocity magnitude on the right.

AboutFlow ITN. The flow is turbulent, with a $Re = 3000$ based on the inlet hydraulic diameter and the Spalart-Allmaras turbulence model is used along with its adjoint, as presented in section 2. $J_{p_t}$ is used as the objective function and reduced by $\sim 50\%$, under the $C$ constraint with $t = 0.7$. The $I_{B-P}$ function was used in eqs. 1b to 1d together with a regularization of the porosity field. TopO blocks the areas of the initial domain with a high flow recirculation, minimizing pressure losses significantly.

Finally, fig. 5 presents a CHT TopO of a micro-channel. The bottom and side walls of the

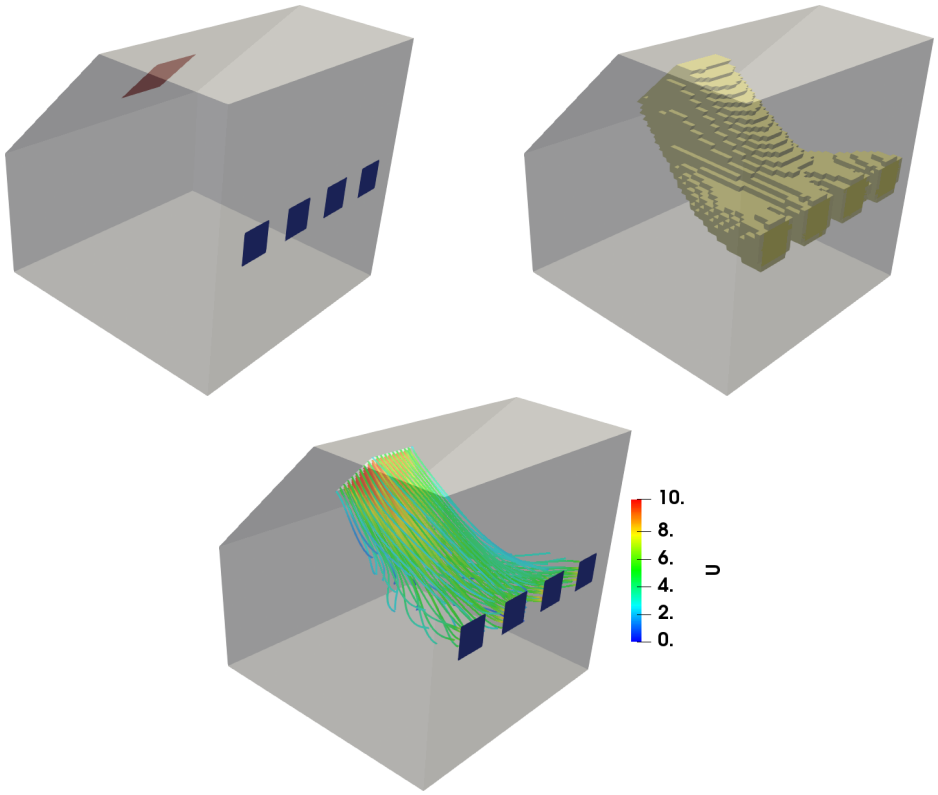


Figure 3: Case 3, 3D manifold. The flow enters the domain from the inlet, coloured in red, and exits from the four outlets, coloured in blue (top-left). The duct walls can be traced by computing a $\beta$ iso-surface of an almost zero value (here an iso-surface of $\beta = 10^{-5}$, coloured in yellow, top-right). The velocity streamlines, coloured by the velocity magnitude are depicted in the bottom sub-figure.

channel have a temperature of $373K$ while the flow enters the domain from the left with $273K$ and a $Re = 166$. The walls adjacent to the inlet and outlet are adiabatic and the top surface has symmetry conditions. Weighted combinations of the $J_{p_t}$ and $J_Q$ objectives are formulated by varying the $w_{p_t}$ and $w_Q$ weights in the following expression $J = w_{p_t} J_{p_t} - w_Q J_Q$ which is then minimized multiple times. For all cases studied, the $C_V$ constraint is also imposed with $t = 0.5$. As expected, the $(w_{p_t}, w_Q) = (1, 0)$ weight value-set leads practically to a straight duct while increasing $w_Q$ leads to the designs of ducts that approach the lower heated wall, in order to heat the flowing fluid. In this case, $I^v = I_{B-P}$, $I^k = I_{SIMP}$ and a regularization and projection strategy was necessary to avoid a checkerboard effect when $w_Q$ was increased. The trade-off between $J_{p_t}$ and $J_Q$ can be seen in fig. 6, where a front on non-dominated solutions has been computed separately by optimizing for a number of $(w_{p_t}, w_Q)$ weight value-sets.

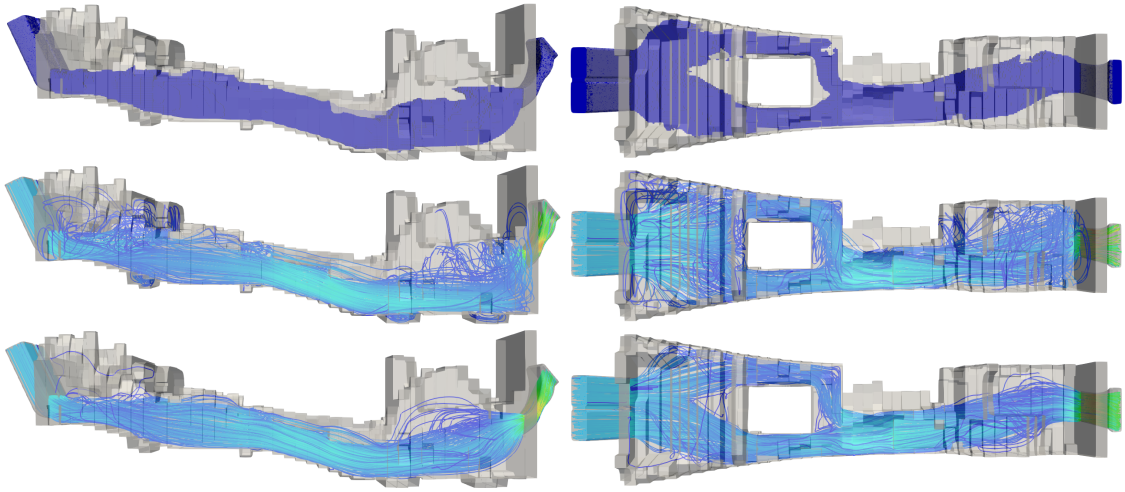

Figure 4: Case 4, HVAC duct. Top: a $\beta$ iso-surface of $10^{-3}$ showcasing the walls designed by TopO, coloured in blue, along with the blurred boundaries of the computational domain, coloured in light grey. Mid and bottom: streamlines of the flow velocity coloured by its magnitude for the baseline and optimized geometries, respectively. It can be seen that by blocking the areas in which the geometry cross-section was increasing abruptly in the baseline design, TopO has reduced a large portion of the initially present recirculation, reducing losses significantly.

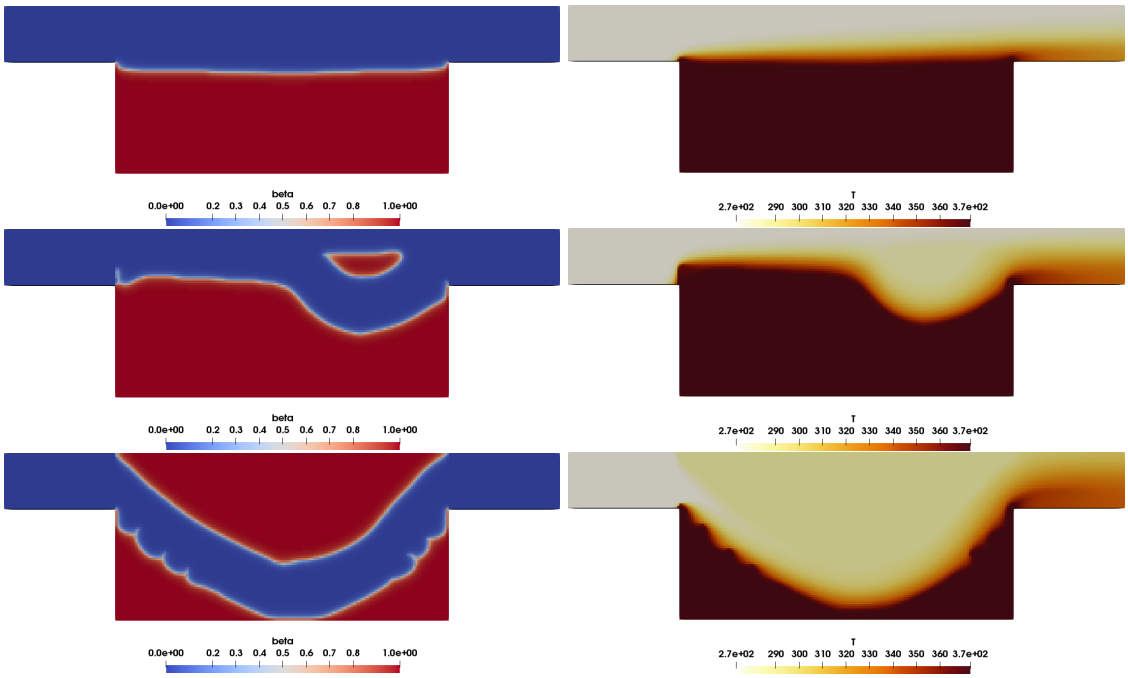


Figure 5: Case 5, CHT optimization of a micro-channel. The $\beta$ distributions for various weight value-sets are depicted on the left while the fluid and solid temperatures are portrayed on the right. From top to bottom, the weight values-sets $(w_{p_t}, w_Q)$ multiplying $J_{p_t}$ and $J_Q$ are (1,0), (0.5,0.5) and (0.1,0.9).

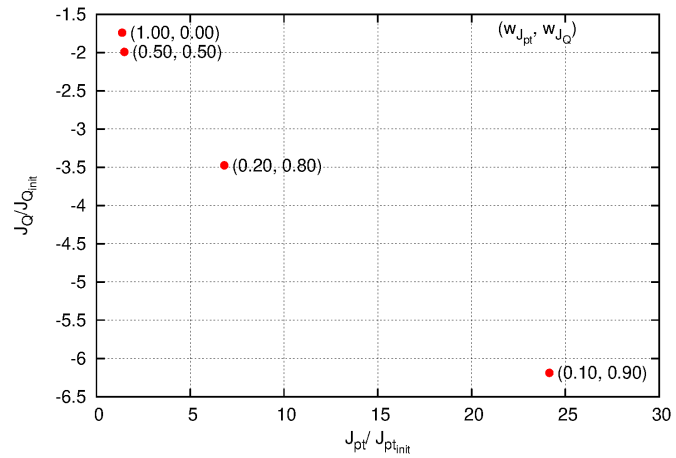


Figure 6: Case 5, CHT optimization of a micro-channel. The front of non-dominated solutions computed by conducting a number of different optimizations, each with a different $(w_{J_{pt}}, w_Q)$ weight value set. All objective values have been normalized with the ones corresponding to the flow and temperature solution with $\beta = 0$.

# 4 Closure

A density-based topology optimization method and software for aero/hydrodynamic as well as conjugate heat transfer problems has been developed by extending the continuous adjoint infrastructure of OpenFOAM v1912/v2006. The software implements a number of features like different interpolation functions, regularization and projection of the porosity field, utilizes (GC)MMA to update the design variables and even borrows ideas from level-set approaches to avoid early entrapment into local minima. Initial testing has showed that the introduction of regularization may decrease the contrast of the porosity field, making the boundaries between the fluid and solid domain slightly more blurry, but is necessary to tackle CHT topology optimization problems in which checkerboard effects are very common. On the contrary, its use is not mandatory in purely aero/hydrodynamic optimization problems. The software was applied to a number of 2D and 3D topology optimization problems, practically replicating the optimized solutions that were computed with an older level-set approach for some of the examined cases. Additionally, new cases were examined, including CHT, highlighting a trade-off between total pressure losses minimization and heat-flux increase.

# References


[1] M. Bendsoe and O. Sigmund. Material interpolation schemes in topology optimization. *Archive of Applied Mechanics*, 69:635–654, 1999.

[2] T. Borvall and J. Peterson. Topology optimization if fluids in stokes flow. *International Journal for Numerical Methods in Fluids*, 41:77–107, 2003.

[3] C.B. Dilgen, S.B. Dilgen, D.R. Fuhrman, O. Sigmund, and B.S. Lazarov. Topology optimization of turbulent flows. *Computer Methods in Applied Mechanics and Engineering*, 331:363 – 393, 2018.

[4] J.R.L. Koch, E.M. Papoutsis-Kiachagias, and K.C. Giannakoglou. Transition from adjoint level set topology to shape optimization for 2D fluid mechanics. *Computers & Fluids*, 150:123–138, 2017.

[5] B.S. Lazarov and O. Sigmund. Filters in topology optimization based on Helmholtz-type differential equations. *International Journal for Numerical Methods in Engineering*, 86(6):765–781, 2011.

[6] L. Olesen, F. Okkels, and H. Bruus. A high-level programming-language implementation of topology optimization applied to steady-state Navier-Stokes flow. *International Journal for Numerical Methods in Engineering*, 65:975–1001, 2006.

[7] C. Othmer. Adjoint methods for car aerodynamics. *Journal of Mathematics in Industry*, 4(6), 2014.

[8] E.M. Papoutsis-Kiachagias and K.C. Giannakoglou. Continuous adjoint methods for turbulent flows, applied to shape and topology optimization: Industrial applications. *Archives in Computational Methods in Engineering*, 32(2):255–299, 2016.

[9] P. Spalart and S. Allmaras. A one-equation turbulence model for aerodynamic flows. AIAA Paper 1992-439, 30th Aerospace Sciences Meeting and Exhibit, Reno, Nevada, USA, January 6–9 1992.

[10] K. Svanberg. The method of moving asymptotes – a new method for structural optimization. *International Journal for Numerical Methods in Engineering*, 24(2):359–373, 1987.

[11] K. Svanberg. A class of globally convergent optimization methods based on conservative convex separable approximations. *SIAM Journal on Optimization*, 12(2):555–573, 2002.

[12] A.S. Zymaris, D.I. Papadimitriou, K.C. Giannakoglou, and C. Othmer. Continuous adjoint approach to the Spalart-Allmaras turbulence model for incompressible flows. *Computers & Fluids*, 38(8):1528–1538, 2009.